Sensors and Actuators A 199 (2013) 344–352

Contents lists available at SciVerse ScienceDirect

Sensors and Actuators A: Physical

journal homepage: www.elsevier.com/locate/sna

A new energy harvester design for high power output at low frequencies

Lokesh Dhakar[a,b], Huicong Liu[a], F.E.H. Tay[b,c], Chengkuo Lee[a,*]

[a] Department of Electrical and Computer Engineering, National University of Singapore, 4 Engineering Drive 3, Singapore 117576, Singapore
[b] NUS Graduate School for Integrative Sciences and Engineering, 28 Medical Drive, Singapore 117456, Singapore
[c] Department of Mechanical Engineering, National University of Singapore, 9 Engineering Drive 1, Singapore 117576, Singapore

ARTICLE INFO

Article history:
Received 16 March 2013
Received in revised form 7 June 2013
Accepted 7 June 2013
Available online xxx

Keywords:
Energy harvester (EH)
Low frequency
High power output
Composite cantilever beam
Mechanical stopper
Bandwidth widening

ABSTRACT

The energy harvesters (EHs) using resonant mechanism have encountered two major issues: low output power scavenged from low frequency vibrations, and limited effectiveness of harvesting mechanism in a narrow range near resonant frequency. To overcome these issues, we have proposed a piezoelectric EH comprising a composite cantilever and a proof mass at the free end. The composite cantilever is formed by a piezoelectric bimorph and a polymer beam (soft spring) mechanically connected along the longitudinal direction. Comparing with the resonant frequency of 275 Hz of a standalone piezoelectric bimorph, the composite cantilever design enables the resonant frequency of the EH to be as low as 36 Hz. Moreover, this kind of EH is demonstrated to be 3.12 times and 1.32 times (at 0.1 g) more efficient at output power generation than a standalone piezoelectric bimorph and piezoelectric bimorph with a proof mass at the free end, respectively. With the aid of spring hardening effect, the operating bandwidth (BW) can be increased from 5 Hz to 16.4 Hz.

1. Introduction

Energy harvesting has become an active field of research in past few years and has showed tremendous applications in many areas including implantable biosensors [1], consumer electronics [2,3], military equipment [4] and wireless sensor networks (WAN) [5–9]. Vibration based energy harvesting [10] is an alternative to solar and thermoelectric energy harvesting for scenarios where sun and thermal gradients are not readily present. These EHs are designed to convert the vibrational energy available in the environment into usable form to power small electronic devices and eliminate the expense and inconvenience involved in replacing the batteries periodically. To harvest ambient vibration energy, piezoelectric [6], electromagnetic [7] and electrostatic [8] approaches have been used by the researchers. Among these approaches, piezoelectric EHs have garnered more attention because of its high power conversion efficiency and simple operating mechanism [11–14]. Most of the reported piezoelectric EHs working on resonance based mechanism typically use simple piezoelectric cantilever structure and incorporate proof mass [15,16] to increase the average strain in the piezoelectric layer [17] and thus enhance the power output.

The frequency of ambient vibration sources, such as household equipment, buildings [11], human body motion [12] and heart beat [13], are typically less than 100 Hz. Therefore, it is necessary to bring down the resonant frequency of EHs to match the ambient excitation frequency. As the size of the energy harvesting device decreases to a smaller form factor, the resonant frequency of the device increases which makes it difficult to harvest low frequency vibrations less than 100 Hz. The traditional solution for reducing the resonant frequency of the EHs is to attach a proof mass at the free end of the cantilever. Liu et al. [14] used an S-shaped beam with a proof mass to achieve low frequency operating range of less than 30 Hz. But the new beam shape results in a decrement in the effective piezoelectric film area. On the other hand, a vibrational EH has a very limited operating bandwidth (BW) nearby its resonant frequency. To solve the narrow BW issue, Sari et al. [18] reported an array of cantilevers with different dimensions and resonant frequencies. The array of 35 cantilevers produced an overall voltage and power output of 10 mV and 0.4 μW, respectively, within a wide BW of 800 Hz (4.2–5 kHz). Eichhorn et al. [19] demonstrated a frequency tuning approach by the application of an axial force at the free end of a cantilever beam. Challa et al. [20] realized frequency tuning by applying a magnetic force on a cantilever in the transverse direction. Nguyen et al. [21] used electrostatic micromechanical non-linear springs under colored noise vibrations which resulted in a wideband operating range. Soliman et al. [22] and Liu et al. [23,24] used amplitude limiter or mechanical stopper which converted a

* Corresponding author. Tel.: +65 6516 5865; fax: +65 6779 1103.
E-mail address: elelc@nus.edu.sg (C. Lee).

0924-4247/$ – see front matter © 2013 Elsevier B.V. All rights reserved.
http://dx.doi.org/10.1016/j.sna.2013.06.009

Nomenclature

k_1	spring constant of the piezoelectric bimorph
k_2	spring constant of the polymer beam
k_{eff}	effective spring constant of composite beam
m_p	proof mass
m_e	effective mass of the cantilever at end
f	resonant frequency for the first mode of the oscillator
R	radius of curvature of the beam
l_1	length of piezoelectric bimorph
l_2	length of polymer beam
Y_s	Young's modulus of substructure in bimorph
Y_{piezo}	Young's modulus of piezoceramic
Y_{poly}	Young's modulus of polymer
I_{piezo}	area moment of inertia of piezoelectric part
I_{sub}	area moment of inertia of substructure part
ρ_{piezo}	density of piezoceramic
ρ_{poly}	density of polymer
w_1	width of piezoelectric bimorph
w_2	width of polymer beam
t_1	thickness of piezoelectric bimorph
t_2	thickness of polymer beam
h_{piezo}	height of piezoelectric layer in bimorph
h_{sub}	height of brass substructure in bimorph
d	distance between stopper and proof mass
h	height of proof mass above the centerline of composite cantilever
D_i	electric field displacement in 'i' direction
E_i	electric field in 'i' direction
F_t	force at the end of the piezoelectric bimorph
M_t	moment at the end of piezoelectric bimorph
T_i	stress in the 'i' direction
ξ_i	strain in the 'i' direction
s_{ij}	components of the compliant matrix
$\varepsilon_0\varepsilon_{33}^T$	z-component of dielectric permittivity of piezoelectric layer at a constant stress
V_{oc}	open circuit voltage generated by single piezoelectric layer
Z_p	impedance of single piezoelectric layer in bimorph
Z_L	load resistance connected to the bimorph
P_{av}	average output power transferred to the load resistor
δ_1	deflection at the end of the piezoelectric bimorph
I	current in the energy harvester circuit
P_{av}	average power transferred to load resistor

linear oscillator into a piecewise linear oscillator for a widened BW characteristics. Stanton et al. [25] demonstrated a wideband piezoelectric EH which invoked both hardening and softening effect in the EH by tuning nonlinear magnetic interactions. Arrieta et al. [26] proposed a device using a bistable composite plate with bonded piezoelectric patches for broadband non-linear energy harvesting. Galchev et al. [27] demonstrated a parametric frequency increased generator for harvesting low frequency and wideband vibrations. The structure utilized three magnetically coupled structures to induce high frequency oscillations in an electromechanical transducer.

Theoretically, the power output is proportional to the cubic power of resonant frequency of the EH [28] for a constant proof mass displacement. This results in a fundamental problem of low power output for a low frequency energy harvester. Hajati and Kim [29] reported a clamped–clamped type beam structure with proof mass in the middle. Due to the non-linear behavior of stretching strain, Duffing stiffening occurred in the reported design, which resulted in increased power output of 45 μW. Guyomar et al. [30] investigated a non-linear processing technique using active materials. They reversed the polarity of charge on a piezoelectric element by ringing the charge through an inductor as the element is in stressed state (at maxima and minima of the displacement). It was demonstrated that this approach resulted in increased voltage and power output. All of these approaches endeavored to increase the power output of EHs either by optimizing mechanical design or the electrical circuit attached to EH. Kulah and Najafi [31] proposed an energy harvester for low frequency energy harvesting which converted low-frequency environmental vibrations to a higher frequency by a mechanical frequency up-converter using a magnet. Liu et al. [32] demonstrated a MEMS based piezoelectric EH by using a high resonant frequency cantilever as a frequency up-conversion stopper. The device achieved a peak power density of 159.4 $\mu W/cm^3$ at an acceleration of 0.8 g at 25 Hz. Lee and Carman [33] used a mechanical scrape through approach between the tip of piezoelectric beam and superelastic ridges for frequency up-conversion to harvest mechanical vibration at low frequencies.

In this paper, to overcome the challenge of low power output at low operating frequency, we present a novel composite cantilever design by connecting a polymer cantilever in series with the piezoelectric bimorph. This design leads to not only low operating frequency but also considerable increment in the power output. This approach demonstrates a simple and effective way to produce more power at low frequencies for the same magnitude of external excitation. Moreover, a stopper is used on one side of a composite cantilever to address the problem of narrow BW problem.

2. Design and prototype

As shown in Fig. 1(a), the proposed piezoelectric EH configuration, termed as PEH-S, consists of a composite cantilever and a proof mass. To form the composite cantilever, a polymer beam (made of polyethylene terephthalate) is firmly clamped to a piezoelectric bimorph (5A Navy Type II piezoceramic [34], Piezo Systems Inc.) in the longitudinal direction with the help of metal strips and epoxy adhesives. At the free end of the polymer beam, a proof mass $m_p = 0.72$ g is attached. The polymer material has a low Young's modulus of 0.5 GPa as compared to 66 GPa of the piezoceramic. The significantly low Young's modulus of the polymer results in a very low spring constant of polymer beam than that of piezoelectric bimorph. To provide mechanical excitation, PEH-S is clamped on an electromagnetic shaker using a simple Perspex clamping setup as shown in Fig. 1(b). In Fig. 1(c), an amplitude stopper is fixed at one side of the composite cantilever to widen the operating BW of PEH-S. The distance between the stopper and the top surface of the proof mass is d, and the height of the proof mass above the centerline of the composite cantilever is h.

Stewart et al. [35] has demonstrated that the maximum energy is generated when the cantilever beam coverage area of the piezoelectric layer is 2/3rd of the total cantilever length, under the assumption of a linear strain distribution in piezoelectric cantilever. Fig. 3 shows the simulation results of the voltage distribution in a simple piezoelectric cantilever under a concentric force at the free end. It depicts that the piezoelectric layer toward free end of cantilever has no contribution in energy generation due to negligible strain, while the part toward the free end reduces the overall power due to a redistribution of charge [35]. Therefore, in our present PEH-S design, the piezoelectric bimorph as the energy generation component, is near the fixed end of the composite cantilever and comprises of 60% of total composite cantilever length. This enables composite cantilever design to efficiently use the high strain region to generate energy. For the comparison of PEH-S, two different

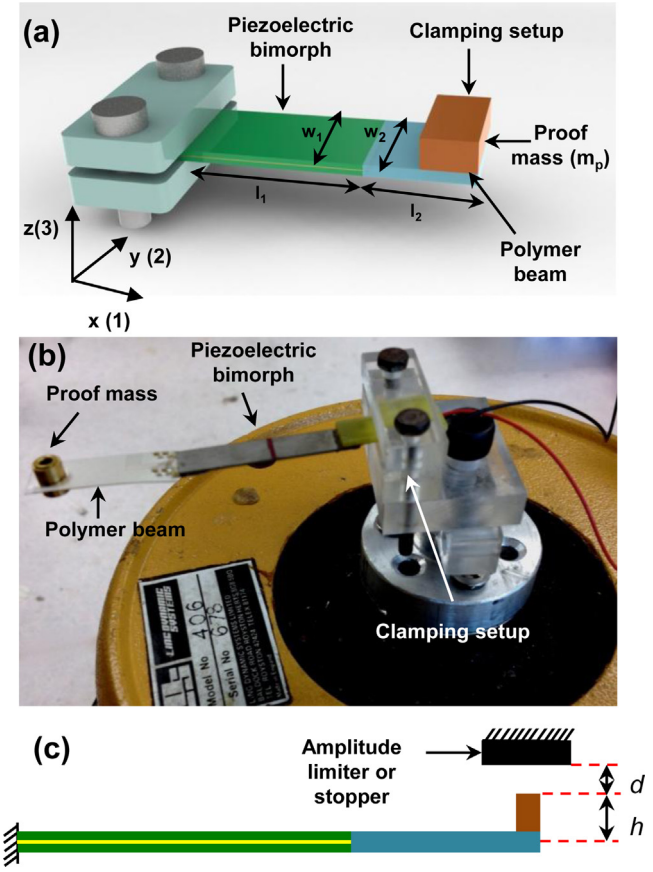

Fig. 1. (a) Design of PEH-S with a polymer spring attached to piezoelectric bimorph. (b) Device prototype assembled on an electromagnetic shaker with different parts marked. (c) Fixed mechanical stopper on one side of PEH-S.

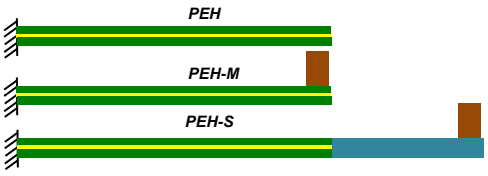

Fig. 2. Three configuration of piezoelectric energy harvesters (PEH, PEH-M and PEH-S).

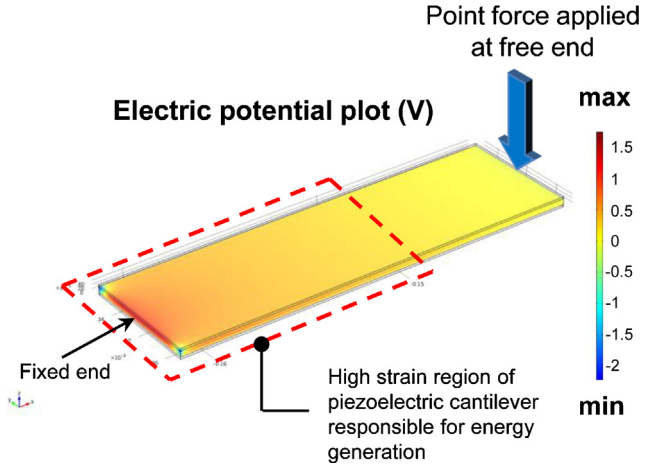

Fig. 3. Simulation results depicting voltage generated in high strain region responsible for energy generation.

Fig. 4. Schematic lumped parameter model of the device used to model frequency characteristic of PEH-S.

prototypes of EHs namely PEH and PEH-M are characterized as well. As shown in Fig. 2, PEH is a similar standalone piezoelectric bimorph as the one used in PEH-S without any proof mass. PEH-M is a similar piezoelectric bimorph with a proof mass of 0.72 g at the end, which is equivalent to the proof mass of PEH-S.

3. Analytical model

3.1. Resonant frequency of the PEH-S system

The resonant frequency of a cantilever with a proof mass at the nth mode is given by [12]:

$$f_n = \frac{\nu'^2_n}{2\pi}\frac{1}{l^2}\sqrt{\frac{k}{m_e + m_p}} \tag{1}$$

where $k = 3EI/l^3$, $I = wt^3/12$ and $\nu'^2_n = \nu^2_n\sqrt{0.236}/3$. w, t and l are the width, thickness and length of the cantilever, respectively. ν_n is the nth mode eigenvalue. For the first mode ($n = 1$), $\nu_n = 1.875$. The value of ν'^2_n is calculated to be 0.986. When a cantilever is modeled as a spring mass system, the governing equation for the first mode resonance of the system can be expressed in the following form:

$$f = \frac{1}{2\pi}\sqrt{\frac{k'}{m_e + m_p}} \tag{2}$$

where $k' = (0.986)^2 k$, m_p is proof mass attached at the free end and m_e is the effective mass of the cantilever at the free end ($m_e = 0.236 \times$ mass of the cantilever). Therefore, the spring constant of a cantilever can be calculated as:

$$k' = \frac{(0.986)^2 3EI}{l^3} = 0.972\frac{3EI}{l^3} \tag{3}$$

where E is the Young's modulus of the cantilever, I is the area moment of inertia and l is the length of the cantilever.

To study the first mode of PEH-S, it is simplified as a lumped parameter spring mass model as shown in Fig. 4. The composite cantilever is modeled as a piezoelectric bimorph of spring constant k_1 and a polymer beam of spring constant k_2 connected in series. The proof mass m_p is attached at the free end. The effective mass of the piezoelectric bimorph and the polymer cantilever is neglected in the model, since it is much smaller than the proof mass m_p. The resonant frequency of the overall system is calculated by the following equation:

$$f = \frac{1}{2\pi}\sqrt{\frac{k_{eff}}{m_p}} \tag{4}$$

The effective spring constant for the composite beam of PEH-S is given by:

$$\frac{1}{k_{eff}} = \frac{1}{k_1} + \frac{1}{k_2} \tag{5}$$

From Eq. (5), if k_2 is much smaller than k_1, then the term $(1/k_2)$ is dominant in determining the effective spring constant of composite beam. Hence it is clear that the softer spring predominantly governs the resonant frequency, and thus results in a low resonant frequency of the overall system. In fact, the dimensions and the material of the soft spring can be further optimized to bring down the operating frequency to even lower levels. The parameters for

Table 1
Parameters for spring k_1.

Parameter	Symbol	Value
Young's modulus	E_{piezo}	6.6×10^{10} Pa
Density	ρ_{piezo}	7800 kg/m^3
Dimensions	$t_1 \times w_1 \times l_1$	.51 mm × 6.4 mm × 31.88 mm

Table 2
Parameters for spring k_2.

Parameter	Symbol	Value
Young's modulus	E_{poly}	500×10^6 Pa
Density	ρ_{poly}	1390 kg/m^3
Dimensions	$t_2 \times w_2 \times l_2$	125 mm × 13.2 mm × 21.33 mm

the spring k_1 and k_2 are given in Tables 1 and 2. Using Eq. (3), the values of the spring constant k_1 and k_2 are obtained to be approximately 423 N/m and 34 N/m, respectively. According to Eq. (2), the resonant frequencies in the first bending mode of PEH and PEH-M are obtained to be 250 Hz and 110 Hz, respectively. However, the resonant frequency of PEH-S is calculated to be 33 Hz using Eq. (4), which is significantly lower compared to PEH and PEH-M.

3.2. Output voltage and averaged power

The piezoelectric constitutive equations [36] define the relationship between stress, strain, electric displacement and electric field for a piezoelectric material. When the piezoelectric layer operates in d_{31} mode, the constitutive equations can be rearranged as Eqs. (6) and (7). The d_{31} mode refers to the situation when an applied stress in $x(1)$ direction induces electrical displacement in $z(3)$ direction. The axes convention is shown in Fig. 1(a).

$$\xi_1 = s_{11}^E T_1 + d_{31} E_3 \tag{6}$$

$$D_3 = d_{31} T_1 + \varepsilon_0 \varepsilon_{33}^T E_3 \tag{7}$$

where ξ_1 is the strain, s_{11} is compliance at constant electric field, d_{31} is the piezoelectric coefficient, E_3 is the electric field, D_3 is the electric displacement, T_1 is the stress vector and $\varepsilon_0 \varepsilon_{33}^T$ is the dielectric permittivity at constant stress. The subscripts 1, 2 and 3 associated with the parameters denote the directions x, y and z, respectively.

In PEH-S, output voltage is generated only due to piezoelectric bimorph part. As shown in Fig. 5, the effect of the polymer beam on the piezoelectric bimorph is modeled using force F_t and moment M_t. F_t is the reaction force exerted due to inertial force of proof mass and M_t is the moment on the bimorph due to this inertial force. The poling directions of two piezoelectric layers connected in parallel are in the same direction. A piezoelectric EH is typically connected with an external electrical circuit components like rectifier, capacitor, resistor, etc. In this work, the piezoelectric layer in the bimorph is modeled as a voltage source with an open circuit voltage V_{oc} and an impedance Z_p in series. A load resistor of magnitude Z_L is connected to PEH-S. Thus the equivalent circuit of PEH-S is a voltage

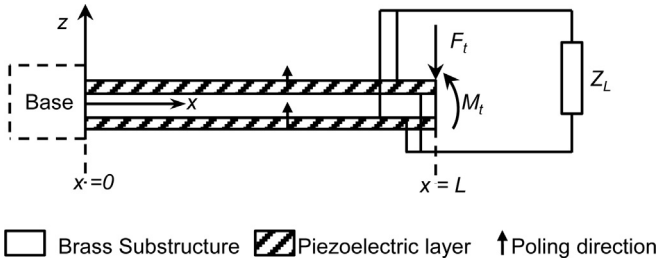

Fig. 5. Diagram representing piezoelectric bimorph with layers in parallel connection.

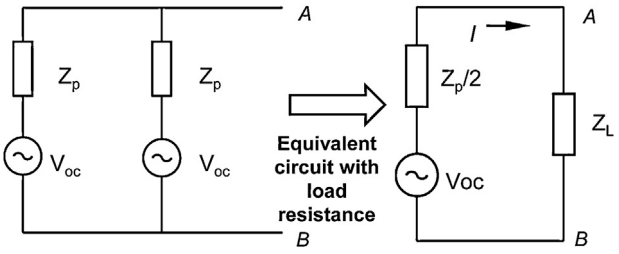

Fig. 6. Equivalent electrical circuit of piezoelectric bimorph.

source V_{oc} and an impedance $Z_p/2$ connected with a load resistance of impedance Z_L (Fig. 6). The current I in the closed circuit can be calculated using Ohm's law for reactive circuits:

$$I = \frac{V_{oc}}{Z_p/2 + Z_L} \tag{8}$$

The average powered transferred to the load resistor can be written as:

$$P_{av} = \frac{1}{2} I^2 Z_L = \frac{1}{2} \frac{V_{oc}^2}{(Z_p/2 + Z_L)^2} Z_L \tag{9}$$

As bimorph can be considered to be a fairly slender structure, Euler–Bernoulli beam theory is applied to obtain strain distribution in the bimorph (Appendix A) as given in Eq. (10).

$$\xi_{1av} = \frac{6\delta_1}{(l_1 + 3l_2) l_1^2} (l_1 + l_2 - x) \left(h_{piezo} + \frac{h_{sub}}{2} \right) \tag{10}$$

The open circuit voltage across the individual piezoelectric layer can be calculated [28] as:

$$V_{oc} = -\frac{Y_{piezo}}{\varepsilon_0 \varepsilon_{33}} \frac{h_{piezo}}{l_1} \int_0^{l_1} \xi_{1av}(x) dx = \frac{6 Y_{piezo}}{\varepsilon_0 \varepsilon_{33}} \frac{h_{piezo}(h_{piezo} + h_{sub}/2)}{l_1^2 (l_1 + 3l_2)} \times \left(\frac{l_1}{2} + l_2 \right) \delta_1 \tag{11}$$

According to the maximum power transfer theorem, the maximum power occurs when the load impedance is equal to the source impedance [37]. Therefore the optimum load resistance for the PEH-S is equal to $|Z_p/2|$. The average power transferred to the optimum load resistance can be calculated as:

$$P_{av} = \frac{1}{2} I^2 Z_L = \frac{1}{2} \frac{V_{oc}^2}{(Z_p)^2} \left(\frac{Z_p}{2} \right) = \frac{1}{4} \frac{V_{oc}^2}{Z_p} \tag{12}$$

3.3. BW widening using mechanical stopper

The BW of PEH-S can be increased by using mechanical stopper as shown in Fig. 1(c). The spring constant variation of the composite cantilever due to stopper is shown in Fig. 7. As the amplitude of the proof mass increases more than d, the stopper halts its motion.

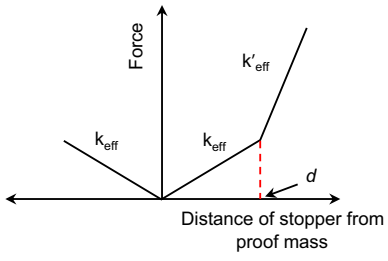

Fig. 7. Variation of effective spring constant with respect to the displacement of proof mass.

Due to stopper, spring stiffening occurs and the effective spring constant increases from k_{eff} to k'_{eff}. In this case, PEH-S can be considered as a piecewise linear oscillator, the equation of motion with dimensionless parameters is given by [24,38]:

$$\ddot{u} + 2\zeta_0\dot{u} + u = r^2 \sin(r\tau) + f_1(u, \dot{u}) \tag{13}$$

where $\omega_0 = 2\pi f_0$; $\omega_1 = 2\pi f_1$; $\tau = \omega_0 t$; $r = \omega/\omega_0$; $r_1 = \omega_1/\omega_0$; $u = z/Y$; $\delta_1 = d/Y$; f_0 and f_1 are the frequency characteristics of PEH-S and stopper, respectively; z is the displacement at the free end of the composite beam; Y is the amplitude of the mechanical excitation provided in the form of $y = Y \sin \omega t$; ζ_0 is the damping ratio for PEH-S. The expression for $f_1(u, \dot{u})$ is given by the following equation:

$$f_1(u, \dot{u}) = \begin{cases} -2r_1\zeta_1\dot{u} - r_1^2 u + r_1^2\delta_1, & u \geq d \\ 0, & u < d \end{cases} \tag{14}$$

where ζ_1 is the damping ratio of stopper; and d is the distance of proof mass from the stopper. The amplitude A of proof mass can be expressed as a function of the dimensionless excitation frequency parameter r as:

$$\pi^2 r^4 = Z_1^2 + Z_2^2 \tag{15}$$

Z_1 and Z_2 are given by the following equations:

$$Z_1 = -2\zeta_0 Ar\pi - r_1\zeta_1 Ar(\pi - 2\varphi_1 - \sin 2\varphi_1) \tag{16}$$

$$Z_2 = \pi A(1 - r^2) - \{0.5r_1^2 A(2\varphi_1 - \sin 2\varphi_1 - \pi) + 2r_1^2\delta_1 \cos \varphi_1\} \tag{17}$$

The frequency response given by Eqs. (13)–(17) is simulated using MATLAB for three different values $d_i = 5.1$ mm, 5.5 mm and 5.9 mm ($i = 1, 2, 3$) at an acceleration of 1 g. In the simulation, the value for ζ_0, ζ_1, f_0 and f_1 are assumed to be 0.02, 0.12, 28 Hz and 150 Hz, respectively. The simulation result is shown in Fig. 8. The proof mass initially moves freely and follows the frequency response of a linear oscillator without stopper from point p to q_i. Once the proof mass moves more than d_i, it engages with the stopper and the effective stiffness and damping coefficient increases. Then the motion of the free end follows the piecewise linear model from point q_i to r_i. After reaching point r_i, the displacement abruptly decreases and returns back to point s_i and follows the frequency response of that without any stopper from point s_i to point t. For more details about the theoretical explanation of the frequency response of the piecewise linear oscillator model, it is referred to [38].

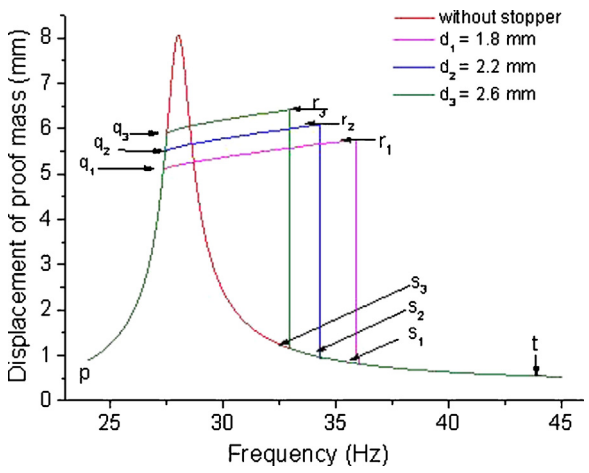

Fig. 8. Simulated frequency responses of EH with stopper at one side for $d = 1.8$ mm, 2.2 mm and 2.6 mm.

4. Experiments and discussion

The experimental setup used for the dynamic characterization of the three EH configurations (PEH, PEH-M and PEH-S) is shown in Fig. 9. The main components are dynamic signal analyzer (DSA), electromagnetic shaker and accelerometer. The DSA (Model no: HP 35670A) acts as a signal source applied to the shaker and the output signal obtained from the EH are acquired by the DSA through Channel 1. The resistance of the DSA is 1 MΩ, so the measured voltage by the DSA is actually the voltage across a load resistance of 1 MΩ. The accelerometer (Brüel & Kjær, Type 4371) mounted on the shaker (Linc Dynamic Systems, Model No. 406) is used to measure the acceleration of the driving vibration, which is then sent to the DSA through Channel 2. To evaluate the frequency responses of EH sine sweep was performed. For power response, rms output voltage measurements were conducted at different load resistance. The measured output voltage was then used to calculate the power across the load resistor.

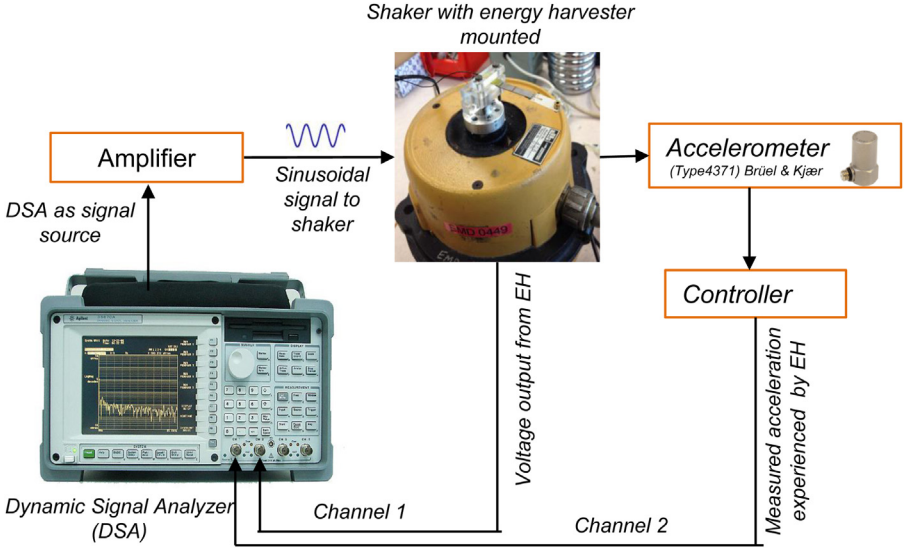

Fig. 9. Schematic diagram of the experimental setup for EHs.

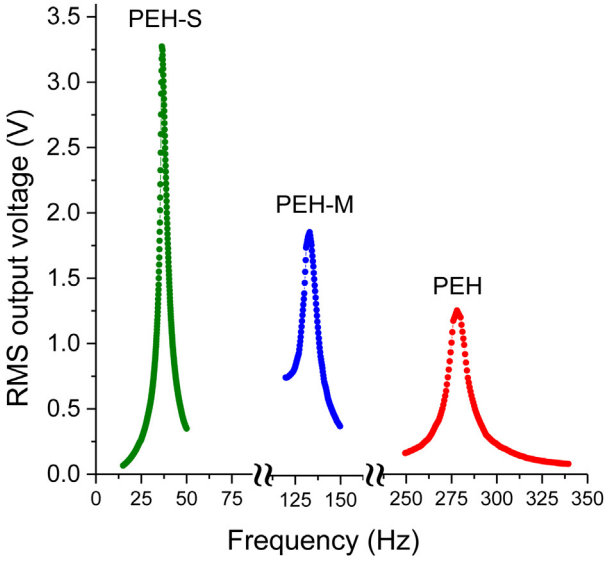

Fig. 10. Frequency responses of PEH, PEH-M and PEH-S at acceleration of 0.2 g.

4.1. Frequency response

The frequency responses of all three configurations at an acceleration of 0.2 g are shown in Fig. 10. The resonant frequencies of PEH, PEH-M and PEH-S are experimentally obtained to be 275 Hz, 125 Hz and 36 Hz, respectively. By using a proof mass at the end of the piezoelectric bimorph, the resonant frequency of PEH-M decreases by a factor of 2.2 compared to PEH. Furthermore, by connecting a polymer cantilever with proof mass, the resonant frequency of PEH-S decreases by a factor of 7.6 and 3.47 compared to PEH and PEH-M, respectively. The output voltages of PEH, PEH-M and PEH-S at the resonant frequency are 1.25 V, 1.9 V and 3.3 V, respectively. The output voltage of PEH-S is significantly improved as compared to PEH-M. As the impedance of a piezoelectric EH is a function of frequency, the optimum load resistance and hence optimum power generated is dependent on resonant frequency. Therefore one more set of experiments were conducted to compare the power output of all three configurations. The results are discussed in the next section.

4.2. Power output comparison for three configurations

A comparative study was conducted for the power output of three configurations (PEH, PEH-M and PEH-S) at two different acceleration levels (0.1 g and 0.2 g). The maximum power occurs when the load resistance matches with the impedance of EH. As shown in Fig. 11a, the maximum power of PEH, PEH-M and PEH-S at an acceleration of 0.1 g is 4.1 μW, 9.7 μW and 12.8 μW, respectively. At an acceleration of 0.2 g maximum power output is found to be 15 μW, 35 μW and 40 μW for PEH, PEH-M and PEH-S, respectively (Fig. 11(b)). From the measurement results, at a low operating frequency of 36 Hz of PEH-S compared to 125 Hz of PEH-M, the power output of PEH-S is increased by 32% and 14% at 0.1 g and 0.2 g respectively than those of PEH-M. It can be seen that, by integrating with the polymer beam as soft spring, PEH-S is able to harvest more energy at an extremely low operating frequency of 36 Hz as compared to PEH and PEH-M.

4.3. Widening of BW

The BW widening effect of PEH-S by employing mechanical stopper as shown in Fig. 1(c) was studied at a constant acceleration of 1 g (Fig. 12). Table 3 shows the operating BW and voltage levels of

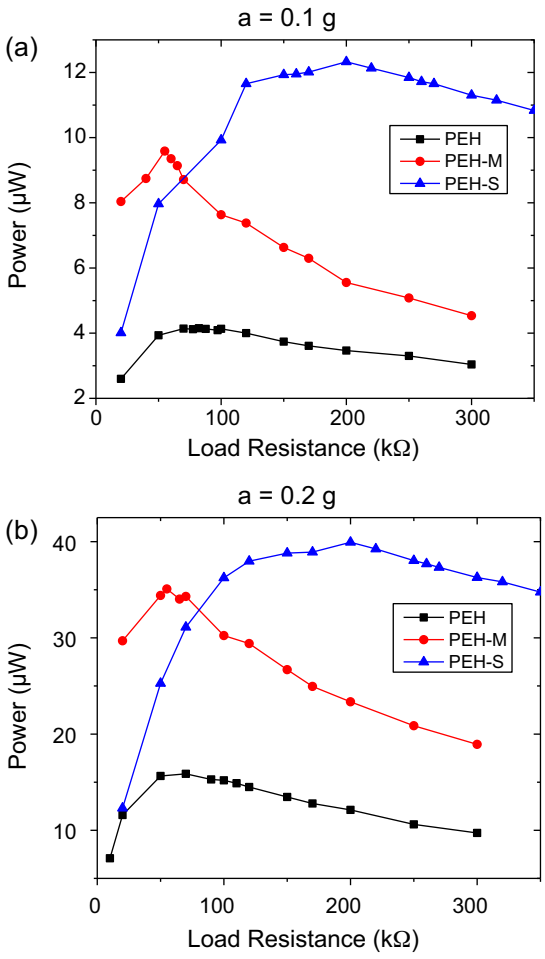

Fig. 11. Power output comparison of three configurations of EH at acceleration (a) 0.1 g and (b) 0.2 g.

PEH-S at different stopper positions. The BW without stopper is calculated at the same voltage level after which the stopper restricts the increase in voltage output. The percentage change in BW is calculated by taking the difference between the operating BWs with and without stopper and dividing it by the operating BW without stopper. For d = 1.8 mm, 2.2 mm and 2.6 mm, operating BW is 8.8 Hz, 6.9 Hz and 5.2 Hz, respectively (Table 3). As the value of d increases,

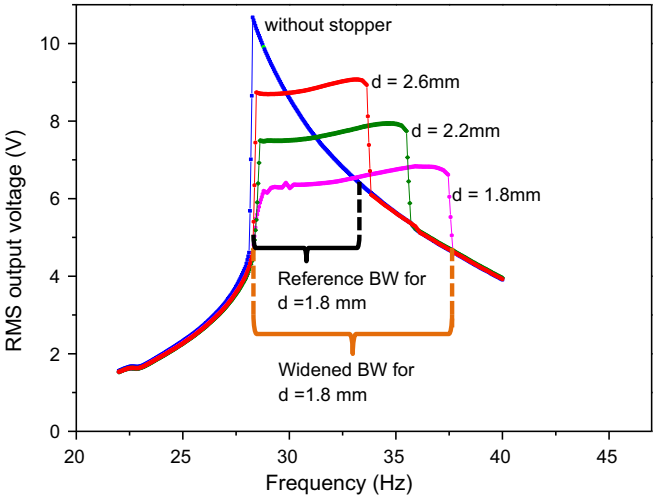

Fig. 12. BW widening of PEH-S at 1 g using stopper at one side at different positions.

Table 3
Operating frequency BW for different stopper positions.

Stopper distance from proof mass (d) (mm)	Voltage level (V)	Operating BW with stopper (Hz)	Operating BW without stopper (Hz)	Percentage change
1.8	6.2	28.7–37.5	28.2–33.2	76%
2.2	7.5	28.6–35.5	28.2–31.3	122.5%
2.6	8.7	28.4–33.6	28.3–29.9	225%

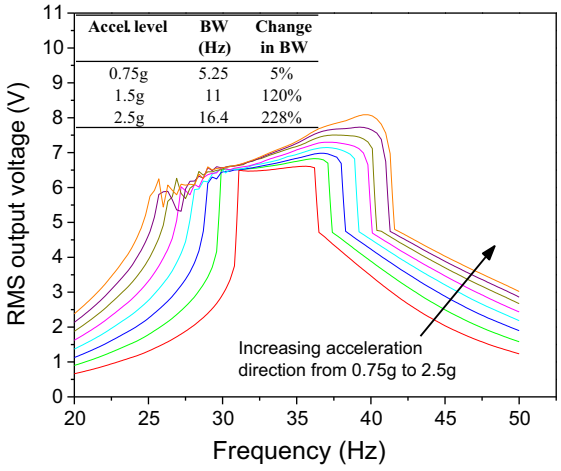

Fig. 13. Variation of the BW of energy harvester with increase in the mechanical excitation level for $d = 1.8$ mm.

the maximum output voltage increases due to the increment in the maximum allowed amplitude. But the operating BW decreases as the value of d increases. The experimental results show the same characteristic behavior as obtained with the analytical simulation for one-sided stopper.

Tests were also conducted to study the effect of acceleration level on operating BW for a fixed value of d. Fig. 13 illustrates the variation of operating BW as the acceleration changes (the arrow depicts the direction of increasing acceleration). For a constant value of $d = 1.8$ mm, the acceleration was varied from 0.75 g to 2.5 g with steps of 0.25 g. Inset table in Fig. 13 shows the percentage changes in the operating BW at 0.75 g, 1.5 g and 2.5 g are 5%, 120% and 228%, respectively. The reference BW for calculating the percentage change is taken as 28.2–33.2 Hz, which is the BW at $d = 1.8$ mm without using stopper at 1 g. As the acceleration increases from 0.75 g to 2.5 g, the BW increases from 5.25 Hz to 16.4 Hz.

5. Conclusion

In this work, a new PEH-S configuration with high power output has been proposed for low-frequency piezoelectric energy harvesting. The power output of PEH-S increases by 32% at 0.1 g while the resonant frequency is decreased by a factor of 3.47, as compared to PEH-M. Widening of operating BW for PEH-S has been achieved from 5 Hz to 16.4 Hz by using mechanical stopper on one side of the cantilever. As the stopper distance between the stopper and PEH-S decreases, the operating BW of PEH-S increases but at the cost of low output voltage level. The operating BW also increases as the acceleration level is increased for a fixed stopper position.

The new composite cantilever design has shown to be promising to reduce the resonant frequency with a significant increase in the overall output power. The proposed design efficiently uses the high strain region to enhance the overall power output. It provides an effective approach to overcome the limitation of low resonant frequency and low power output. It also has potential to be applied to MEMS devices to reduce the resonant frequency of device by using soft springs e.g. serpentine spring or soft materials with low Young's modulus. Optimizing the dimensions of the polymer cantilever is expected to further reduce the resonant frequency.

Acknowledgements

This work is partially supported by the Faculty Research Committee (FRC) Grant (No. R-263-000-692-112) at the National University of Singapore, and the NRF2011 NRF-CRP001-057 Program—'Self-powered body sensor for disease management and prevention-orientated healthcare' (R-263-000-A27-281) from the National Research Foundation (NRF), Singapore.

Appendix A. Modeling of the strain distribution

To determine strain at a distance z from the neutral axis of the beam, an elemental layer is considered at a distance z from the neutral axis of the beam as shown in Fig. A.1a. The neutral axis in the case of a symmetrical bimorph, is the centerline of the substructure as depicted in Fig. A.1b. The initial length of the elemental layer is x and the length after bending is $x + \Delta x$. The change in the length of the elemental layer can be calculated by the following expression:

$$\Delta dx = (R + z)d\theta - Rd\theta \tag{A.1}$$

where $d\theta$ is the angle enclosed by the element chosen as shown in Fig. A.1b, R is the radius of curvature of the bended bimorph at the location of element chosen, z is the distance of the elemental layer from the neutral axis of the bimorph, Δdx is the change in the length of the elemental layer with initial length dx. Eq. (A.2) can be used to calculate the stress at a distance z from the neutral bending axis. The strain ξ_1 in x-direction in bimorph is a function of two x

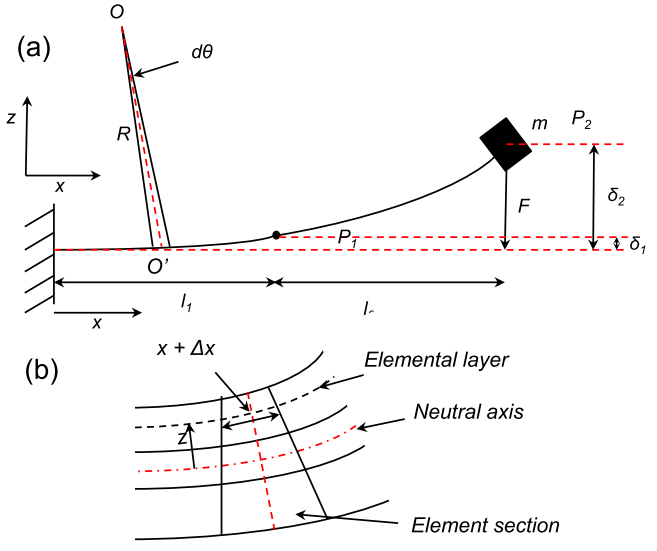

Fig. A.1. (a) Parameters for PEH-S for calculation of strain distribution in piezoelectric bimorph. (b) Element section indicating the elemental layer considered for strain distribution calculation using beam theory.

and z coordinates. The strain at a point with coordinates (x, z) is calculated as:

$$\xi_1(x,z) = \frac{\Delta dx}{dx} = \frac{zd\theta}{Rd\theta} = \frac{z}{R} \tag{A.2}$$

When the piezoelectric bimorph is considered as shown in 5, the force and moment acting at the end of bimorph can be calculated by Eqs. (A.3) and (A.4).

$$F_t = m_p a \tag{A.3}$$

$$M_t = m_p a l_2 \tag{A.4}$$

where a is the excitation acceleration; l_2 is the length of the polymer beam and m_p is the proof mass. According to the Euler–Bernoulli beam theory, the equation of motion for bimorph can be written as:

$$\overline{EI}\frac{d^2z}{dx^2} = m_p a l_2 + m_p a(l_1 - x) \tag{A.5}$$

where $\overline{EI}$ is the equivalent Young's modulus of bimorph and is equal to $E_{piezo}I_{piezo} + E_{sub}I_{sub}$; l_1 and l_2 are the length of piezoelectric bimorph and polymer cantilever, respectively; E_{piezo} and E_{sub} are Young's modulus of piezoelectric layer and substructure layer, respectively; I_{piezo} and I_{sub} are second moment of area for piezoelectric and substructure part, respectively. Integrating the Eq. (A.5) leads to Eq. (A.6). This expression delineates the profile of bimorph when it is bended.

$$z = \frac{m_p a}{\overline{EI}}\left[\frac{l_1 + l_2}{2} - \frac{x}{6}\right]x^2 \tag{A.6}$$

The expression for the term $m_p a/\overline{YI}$ can be calculated in terms of the deflection at the end of piezoelectric bimorph (Point P1 (Fig. A.1a)), which is denoted as δ_1.

$$\delta_1 = z(x = l_1) = \frac{m_p a}{12\overline{EI}}(l_1 + 3l_2)l_1^2 \tag{A.7}$$

Now, the variation of strain in x-direction (ξ_1) can be given by:

$$\xi_1(x,z) = \frac{z}{R} = \frac{m_p a}{\overline{EI}}(l_1 + l_2 - x)z \tag{A.8}$$

Using Eqs. (A.7) and (A.8), the variation of ξ_1 can be written as:

$$\xi_1(x,z) = \frac{12\delta_1}{(l_1 + 3l_2)l_1^2}(l_1 + l_2 - x)z \tag{A.9}$$

The stress in the piezoelectric layer is a function of the coordinates x and z. The electric displacement field in the piezoelectric layer depends on the strain. So for the calculation of the average electric displacement field D_3 induced in the piezoelectric layer, we calculate the average value of the strain along the z-axis as in Eq. (A.10). The strain is now expressed as only a function of x-coordinate:

$$\xi_{1av}(x) = \frac{1}{h_{peizo} - (h_{sub}/2)}\int_{h_{sub}/2}^{h_{piezo}} \xi_1(x,z)dz = \frac{12\delta_1}{(l_1 + 3l_2)l_1^2}(l_1 + l_2 - x) \times \frac{1}{h_{piezo} - (h_{sub}/2)}\int_{h_{sub}/2}^{h_{piezo}} zdz = \frac{6\delta_1}{(l_1 + 3l_2)l_1^2}(l_1 + l_2 - x) \times \left(h_{piezo} + \frac{h_{sub}}{2}\right) \tag{A.10}$$

where h_{piezo} and h_{sub} are height of piezoelectric layer and brass substructure, respectively.

References

[1] M. Rasouli, L.S.J. Phee, Energy sources and their development for application in medical devices, Expert Review of Medical Devices 7 (2010) 693–709.
[2] P. Mitcheson, E. Yeatman, G. Rao, Energy harvesting from human and machine motion for wireless electronic devices, Proceedings of the IEEE 96 (2008) 1457–1486.
[3] J. Paradiso, T. Starner, Energy scavenging for mobile and wireless electronics, Pervasive Computing, IEEE 4 (2005) 18–27.
[4] S.R. Anton, D.J. Inman, Vibration energy harvesting for unmanned aerial vehicles, Proceedings of SPIE 6928 (2008), 692824-692824-12.
[5] C. Enz, A. El-Hoiydi, J. Decotignie, WiseNET: an ultralow-power wireless sensor network solution, Computer 37 (2004) 62–70.
[6] S. Roundy, P.K. Wright, A piezoelectric vibration based generator for wireless electronics, Smart Materials and Structures 13 (2004) 1131.
[7] B. Yang, C. Lee, W. Xiang, J. Xie, J.H. He, R.K. Kotlanka, et al., Electromagnetic energy harvesting from vibrations of multiple frequencies, Journal of Micromechanics and Microengineering 19 (2009) 35001.
[8] S. Meninger, J.O. Mur-Miranda, R. Amirtharajah, A. Chandrakasan, J.H. Lang, Vibration-to-electric energy conversion, IEEE Transactions on Very Large Scale Integration (VLSI) Systems 9 (2001) 64–76.
[9] S. Tadigadapa, K. Mateti, Piezoelectric MEMS sensors: state-of-the-art and perspectives, Measurement Science and Technology 20 (2009) 92001.
[10] S.P. Beeby, M.J. Tudor, N.M. White, Energy harvesting vibration sources for microsystems applications, Measurement Science and Technology. 17 (2006) R175–R195.
[11] S. Roundy, P.K. Wright, J. Rabaey, A study of low level vibrations as a power source for wireless sensor nodes, Computer Communications 26 (2003) 1131–1144.
[12] C.R. Saha, T. O'Donnell, N. Wang, P. McCloskey, Electromagnetic generator for harvesting energy from human motion, Sensors and Actuators A: Physical 147 (2008) 248–253.
[13] M. Amin Karami, D.J. Inman, Powering pacemakers from heartbeat vibrations using linear and nonlinear energy harvesters, Applied Physics Letters 100 (2012) 042901.
[14] H. Liu, C. Lee, T. Kobayashi, C.J. Tay, C. Quan, A new S-shaped MEMS PZT cantilever for energy harvesting from low frequency vibrations below 30 Hz, Microsystem Technologies 18 (2012) 497–506.
[15] K.A. Cook-Chennault, N. Thambi, A.M. Sastry, Powering MEMS portable devices—a review of non-regenerative and regenerative power supply systems with special emphasis on piezoelectric energy harvesting systems, Smart Materials and Structures 17 (2008) 43001.
[16] D. Shen, J.-H. Park, J. Ajitsaria, S.-Y. Choe, H.C. Wikle, D.-J. Kim, The design, fabrication and evaluation of a MEMS PZT cantilever with an integrated Si proof mass for vibration energy harvesting, Journal of Micromechanics and Microengineering 18 (2008) 055017.
[17] S. Roundy, E.S. Leland, J. Baker, E. Carleton, E. Reilly, E. Lai, et al., Improving power output for vibration-based energy scavengers, IEEE Pervasive Computing 4 (2005) 28–36.
[18] I. Sari, T. Balkan, H. Kulah, An electromagnetic micro power generator for wideband environmental vibrations, Sensors and Actuators A 146 (2008) 405–413.
[19] C. Eichhorn, F. Goldschmidtboeing, P. Woias, Bidirectional frequency tuning of a piezoelectric energy converter based on a cantilever beam, Journal of Micromechanics and Microengineering 19 (2009) 94006.
[20] V.R. Challa, M.G. Prasad, Y. Shi, F.T. Fisher, A vibration energy harvesting device with bidirectional resonance frequency tunability, Smart Materials and Structures 17 (2008) 15035.
[21] D.S. Nguyen, E. Halvorsen, G.U. Jensen, A. Vogl, Fabrication and characterization of a wideband MEMS energy harvester utilizing nonlinear springs, Journal of Micromechanics and Microengineering 20 (2010) 125009.
[22] M.S.M. Soliman, E.M. Abdel-Rahman, E.F. El-Saadany, R.R. Mansour, A wideband vibration-based energy harvester, Journal of Micromechanics and Microengineering 18 (2008) 115021.
[23] H. Liu, C.J. Tay, C. Quan, T. Kobayashi, C. Lee, Piezoelectric MEMS energy harvester for low-frequency vibrations with wideband operation range and steadily increased output power, Journal of Microelectromechanical Systems 20 (2011) 1131–1142.
[24] H. Liu, C. Lee, T. Kobayashi, C.J. Tay, C. Quan, Investigation of a MEMS piezoelectric energy harvester system with a frequency-widened-bandwidth

mechanism introduced by mechanical stoppers, Smart Materials and Structures 21 (2012) 035005.
[25] S.C. Stanton, C.C. McGehee, B.P. Mann, Reversible hysteresis for broadband magnetopiezoelastic energy harvesting, Applied Physics Letters 95 (2009) 174103.
[26] A.F. Arrieta, P. Hagedorn, A. Erturk, D.J. Inman, A piezoelectric bistable plate for nonlinear broadband energy harvesting, Applied Physics Letters 97 (2010) 104102.
[27] T. Galchev, E. Aktakka, K. Najafi, A piezoelectric parametric frequency increased generator for harvesting low-frequency vibrations, Journal of Microelectromechanical Systems 21 (2012) 1311–1320.
[28] T.M. Kamel, R. Elfrink, M. Renaud, D. Hohlfeld, M. Goedbloed, C. de Nooijer, et al., Modeling and characterization of MEMS-based piezoelectric harvesting devices, Journal of Micromechanics and Microengineering 20 (2010) 105023.
[29] A. Hajati, S.-G. Kim, Ultra-wide bandwidth piezoelectric energy harvesting, Applied Physics Letters 99 (2011) 083105.
[30] D. Guyomar, A. Badel, E. Lefeuvre, Toward energy harvesting using active materials and conversion improvement by nonlinear processing, IEEE Transactions on Ultrasonics, Ferroelectrics, and Frequency Control and Frequency Control 52 (2005) 584–595.
[31] H. Kulah, K. Najafi, Energy scavenging from low-frequency vibrations by using frequency up-conversion for wireless sensor applications, Sensors Journal IEEE 8 (2008) 261–268.
[32] H. Liu, C. Lee, T. Kobayashi, C.J. Tay, C. Quan, Piezoelectric MEMS-based wideband energy harvesting systems using a frequency-up-conversion cantilever stopper, Sensors and Actuators A: Physical 186 (2012) 242–248.
[33] D.-G. Lee, G. Carman, Novel micro vibration energy harvesting device using frequency up conversion, in: Solid-State Sensors, Actuators and Microsystems Conference, 2007. TRANSDUCERS 2007. International, IEEE, 2007, pp. 871–874.
[34] Piezoceramic Materials & Properties. [Online]. Available: http://www.piezo.com/prodmaterialprop.html (accessed 06.02.13).
[35] M. Stewart, P.M. Weaver, M. Cain, Charge redistribution in piezoelectric energy harvesters, Applied Physics Letters 100 (2012) 073901.
[36] A.J. Moulson, J.M. Herbert, Piezoelectric ceramics, in: Electroceramics, John Wiley & Sons, Ltd., Chichester, UK, 2003, pp. 339–410.
[37] H.W. Jackson, Introduction to Electronic Circuits, Prentice-Hall, Englewood Cliffs, N.J., 1959.
[38] A. Narimani, M.E. Golnaraghi, G.N. Jazar, Frequency response of a piecewise linear vibration isolator, Journal of Vibration and Control 10 (2004) 1775–1794.

Biographies

Lokesh Dhakar received his B.E.(Hons.) degree in Mechanical Engineering from Birla Institute of Technology and Science, Pilani in 2010. He worked in the industry as a design engineer from 2010 to 2011. He is currently pursuing his Ph.D. degree from NUS Graduate School of Integrative Sciences and Engineering, National University of Singapore, Singapore. He is also pursuing his MBA from NUS Business School, concurrently. He is keenly interested in entrepreneurship and technology commercialization. He is currently working on energy harvesting devices aimed at powering wireless wearable sensors for healthcare.

Huicong Liu received her B.Eng. and M.Sc. degrees in Department of Mechanical Engineering from University of Science and Technology Beijing, China, in 2006 and 2008, respectively. She received her Ph.D. degree from the Department of Mechanical Engineering, National University of Singapore (NUS) in Jan. 2013. She has been a Research Fellow in Department of Electrical and Computer Engineering of NUS since Jul. 2012 to Jul. 2013. She is currently an associate professor at the Department of Mechanical Engineering of Soochow University, China. Her research interests are vibration-based MEMS energy harvesters and self powered MEMS devices. She is currently working on energy harvesting solutions for wireless wearable biosensors for disease management and prevention-oriented healthcare.

Francis E.H. Tay received his Ph.D. degree from the Massachusetts Institute of Technology in 1996. He is currently an Associate Professor with the Department of Mechanical Engineering, Faculty of Engineering, National University of Singapore. He is the Deputy Director (Industry) of the Center of Intelligent Products and Manufacturing Systems, where he takes charge of research projects involving the industry and the Center. He is the Founding Director of Microsystems Technology Initiatives and had established the Microsystems Technology Specialization. He has been the Medical Device Group Leader in the Institute of Bioengineering and Nanotechnology, Singapore. He was the Technical Advisor in the Micro and Nano Systems Laboratory, Institute of Materials Research Engineering, Singapore. He is also the Principal Investigator for several Agency for Science, Technology, and Research (A*STAR) Projects. His research areas are MEMS, Biotechnology, nanotechnology and wearable devices.

Chengkuo Lee received the M.S. degree in materials science and engineering from National Tsing Hua University, Hsinchu, Taiwan, R.O.C., in 1991, the M.S. degree in industrial and system engineering from Rutgers University, New Brunswick, NJ, in 1993, and the Ph.D. degree in precision engineering from the University of Tokyo, Tokyo, Japan, in 1996. He worked as researcher in the Nanometerscale Manufacturing Science Laboratory at the Research Center for Advanced Science and Technology (RCAST) of the University of Tokyo from 1993 to 1996. He had also worked in the Mechanical Engineering Laboratory, AIST, MITI of Japan as a JST Research Fellow in 1996. Thereafter, he was a Senior Research Staff Member of Microsystems Laboratory, Industrial Technology Research Institute (ITRI), Hsinchu, Taiwan. In September 1997, he joined the Metrodyne Microsystem Corporation, Hsinchu, Taiwan, and established the MEMS device division and the first micromachining fab for commercial purposes in Taiwan. He was the Manager of the MEMS device division between 1997 and 2000. He was an Adjunct Assistant Professor in the Electrophysics Department of National Chiao Tung University, Taiwan, in 1998, and an Adjunct Assistant Professor in the Institute of Precision Engineering of the National Chung Hsing University, Taiwan, from 2001 to 2005. He co-founded Asia Pacific Microsystems, Inc. (APM) Hsinchu, Taiwan, R.O.C., in August 2001, and he became the Vice President of R&D, then later until the end of 2005, the Vice President of optical communication business unit and Special Assistant of CEO in charge of international business and technical marketing for MEMS foundry service at APM, Inc., one of the top 30 MEMS manufacturers in the world. From 2006 to 2009, he has been a senior member of technical staff at the Institute of Microelectronics (IME), A*STAR, Singapore. Currently he is an associate professor at the Dept. of Electrical and Computer Eng. of National University of Singapore, Singapore. He is the co-author of a book in title of "*Advanced MEMS Packaging*", McGraw-Hill, 2010. He has contributed more than 175 international conference papers and extended abstracts, 125 peer-reviewed international journal articles, and 9 US patents in MEMS, Nanophotonics and Nanotechnology fields. More detailed information of his lab could be found at http://www.ece.nus.edu.sg/stfpage/elelc/home.html.